

Multi-state neural networks based upon spin-glasses: a biased overview

D. Bollé

Recent results are reviewed on both the time evolution and retrieval properties of multi-state neural networks that are based upon spin-glass models. In particular, the properties of models with neuron states having Q -Ising symmetry are discussed for various architectures. The main common features and differences are highlighted.

1 Introduction

Artificial neural networks have been widely applied to memorize and retrieve information. During the last number of years there has been considerable interest in neural networks with multistate neurons (see, e.g., [1]–[3] and references cited therein). Basically, such models can function as associative memories for grey-toned or coloured patterns [4], [5] and/or allow for a more complicated internal structure of the retrieval process, e.g., a distinction between the exact location and the details of a picture in pattern recognition and the analogous problem in the framework of cognitive neuroscience [6], a combination of information retrieval based on skills and based on specific facts or data [7], [8].

In analogy with the well-known Hopfield model [9], [10] the models we discuss here are built from spin-glasses (see [11] for the Hopfield model) with couplings defined in terms of embedded patterns through a learning rule. Since one of the aims of these networks is to find back the embedded patterns as attractors of the retrieval process, they are also interesting from the point of view of dynamical systems.

Different types of multi-state spins (=neurons) can be distinguished according to the symmetry of the interactions between the different states. The states of the Q -Ising neuron can be represented by scalars, and the interaction between two neurons can then be written as a function of the product of these scalars. So the Q -states of the neuron can be ordered like a ladder between a minimum and a maximum value, usually taken to be -1 and $+1$. Special cases are $Q = 2$, i.e., the

Hopfield model and $Q = \infty$, i.e., the analogue or graded response neuron. The states of the phasor or clock neuron can be represented by vectors in the complex plane that are placed (equally spaced) on the unit circle. The interaction between two neurons can then be written as a function of the real part of the product of these vectors indicating the state of the two neurons. The Q -Potts neuron states can be represented by $(Q - 1)$ dimensional vectors that are placed on the edges of a regular $(Q - 1)$ dimensional simplex and the interaction between two neurons is then a function of the scalar product of these vectors, which is either $(Q - 1)/Q$ or $1/Q$. For $Q = 2$ the three types of neurons are the same after proper rescaling, and for $Q = 3$ the phasor and the Potts neurons are equivalent.

The neural network models built with these multi-state neurons have an immediate analogon in spin-glass systems (cfr., e.g., [12] and [13], respectively, [14], [15]). Of course, these types of multi-state neurons do not exhaust all possibilities for constructing models. We also mention the recently considered Ashkin-Teller and Blume-Emery-Griffiths neural network models that are based again upon their spin-glass counterparts (see, e.g., [16], respectively, [17] and references therein), because, as we will argue, they are especially relevant for modeling more sophisticated features of real biological networks and/or from an information theoretic point of view.

Besides these neuron states one also needs to specify an architecture indicating how the neurons are connected with each other. Several architectures have been studied in the literature for different purposes. From a practical applications point of view mostly perceptrons or, more general, layered feedforward networks are used since a very long time. Fully connected attractor networks with symmetric couplings, like the Hopfield model, satisfy the detailed balance principle and hence a Hamiltonian can be defined. The behaviour of such a network can then be studied by focusing on this Hamiltonian. An important feature of these attractor networks is the occurrence of feedback [18]. Diluted architectures where only a fraction of the neurons are connected, are relevant both from the biological point of view and to model the breakdown of synaptic couplings causing loss of information. In particular, symmetrically extremely diluted models still allow for a Hamiltonian description but some feedback survives. Asymmetrically extremely diluted models are considered because their dynamics can be solved exactly since there are no feedback correlations.

Finally, one needs to give an explicit learning rule for the couplings (e.g, Hebb [19], pseudo-inverse [20]) or a strategy to find the couplings giving the best performance (Gardner method [21], [22]).

For a more complete overview of the field from a physics point of view we refer to the textbooks [23]–[29], and to [30]–[33].

Here we review some of the most recent results on multi-state neural networks.

In particular, we focus on the models with Q -Ising symmetry, i.e., the Q -Ising network mainly with $Q = 3$, and the Blume-Emery-Griffiths network. Both the dynamical time evolution and the thermodynamic and retrieval properties for these models with various architectures and a Hebb-type learning rule are discussed.

The methods used are standard by now but have to be slightly extended to accommodate the multi-state character of the neuron. First, in order to study the time evolution under parallel updates of the neurons we mainly use the signal-to-noise analysis. There exist different versions of this method in the literature, e.g., [34]–[39] (see [28] for further references), [40], [41].

In more detail, splitting the local field of the model in a signal part from the condensed patterns and a noise part from the rest of the patterns, and employing systematically the law of large numbers (LLN) and the central limit theorem (CLT) we derive the evolution of the distribution of the local field at every time step. This allows us to obtain a recursive scheme for the evolution of the relevant order parameters in the system. The details of this approach depend in an essential way on the architecture because different temporal correlations are possible.

For extremely diluted asymmetric [42]–[51] (and references therein) and layered feedforward architectures [52]–[56] (and references therein) recursion relations are obtained in closed form directly for the relevant order parameters. This has been possible because in these types of networks there are no feedback correlations as time progresses. As a technical consequence the local field contains only Gaussian noise leading to an explicit solution.

For the parallel dynamics of networks with symmetric connections, however, things are quite different [2], [40], [41], [57]–[59] (and references therein). Even for extremely diluted versions of these systems [60]–[63] (and references therein) feedback correlations become essential from the second time step onwards, complicating the dynamics in a nontrivial way. Therefore, explicit results concerning the time evolution of the order parameters for these models have to be obtained indirectly by starting from the distribution of the local field. Technically speaking, both for the symmetrically diluted and fully connected architectures the local field contains both a discrete and a normally distributed part. In both cases this discrete part prevents a closed-form solution of the dynamics for the relevant order parameters. Nevertheless, the development of a recursive scheme is possible in order to calculate their time evolution.

By requiring through these recursion relations that the local field becomes time-independent implying that most of the discrete noise part is neglected, we can obtain stationary equations for the order parameters.

Since no closed-form solution of this dynamics is possible and the results are technically complicated, it is worthwhile to apply an alternative method, the generating functional approach [64], [65] (for a recent review see, e.g., [66] and refer-

ences therein) to solve this feedback dynamics. This approach enables one to find all relevant physical order parameters at any time step via the derivation of the generating functional. Comparing this approach with the signal-to-noise ratio analysis and with numerical simulations it turns out [59] that beyond the third time step of the dynamics the signal-to-noise analysis, as applied in the literature mentioned above is not completely correct for those parameters of the system corresponding to spin-glass behaviour. The full details of this, showing that a technical assumption concerning the feedback correlations is not valid, although it has little effect in most of the retrieval region of the networks, are worked out first for the simpler $Q = 2$ Hopfield model [67] and are beyond the scope of the present overview.

Secondly, the fixed-point equations for the symmetric models, which are governed by an Hamiltonian, can also be derived using thermodynamic replica mean-field theory [11], [68]. This allows us to write down an expression for the free energy and obtain from it fixed-point equations for the order parameters. Thermodynamic and retrieval properties, e.g., the maximal storage capacity, can be discussed through the appropriate phase diagrams. Most results in the multi-state literature treat models with sequential updating in the replica-symmetric approximation, e.g., [69]–[73] (and references therein) for the Q -Ising and [74] for the Blume-Emery-Griffiths model. These works use Hebb-type learning rules for the couplings. To obtain the optimal storage capacity by finding the optimal couplings which give the best performance of the network for a specific set of patterns, the Gardner-approach can be used to these models. This method treats the couplings as dynamical variables and by using a replica analysis the minimal volume fraction of coupling space is calculated ensuring that this specific set of patterns can still be embedded in the network with a certain basin of attraction. Results for multi-state networks with Q -Ising type neurons can be found, e.g., in [75]–[77] (and references therein).

We remark that the Ashkin-Teller neural network briefly mentioned above will not be discussed here. For recent results on this model and its relation to other networks we refer to [78], [79] and to [80].

The rest of this contribution is organized as follows. In Sections 2 and 3 we consider the Q -Ising model, respectively the Blume-Emery-Griffiths (BEG) model. Each Section is divided in 3 subsections. Subsection 1 defines the model, its dynamics, its relevant order parameters and its measures for the retrieval quality. In subsection 2 we use the signal-to-noise analysis in order to derive a recursive scheme for the evolution of the distribution of the local field, leading to recursion relations for the order parameters. The differences between the various architectures are outlined. Subsection 3 discusses the statics of the model describing the phase diagrams, focusing on the retrieval properties. In Section 4 we briefly describe the results of a Gardner approach to these models. Finally, a short conclusion

is given in Section 5.

This review is limited in both scope and length so that some details and/or contributions could not be mentioned. They are referred to, directly or indirectly, in the references.

2 Q -Ising neural networks

2.1 The model

Consider a neural network consisting of N neurons which can take values $\sigma_i, i = 1, \dots, N$ from a discrete set $\mathcal{S} = \{-1 = s_1 < s_2 < \dots < s_Q = +1\}$. The p patterns to be stored in this network are supposed to be a collection of independent and identically distributed random variables (i.i.d.r.v.), $\{\xi_i^\mu \in \mathcal{S}\}, \mu = \{1, \dots, p\}$, with zero mean, $E[\xi_i^\mu] = 0$, and variance $A = \text{Var}[\xi_i^\mu]$. The latter is a measure for the activity of the patterns. We remark that for simplicity we have taken the patterns and the neurons out of the same set of variables but this is no essential restriction. Given the configuration $\boldsymbol{\sigma}_N \equiv \{\sigma_j(t)\}, j = \{1, \dots, N\}$, the local field in neuron i equals

$$h_i(\boldsymbol{\sigma}_N(t)) = \sum_{j=1}^N J_{ij}(t)\sigma_j(t) \quad (1)$$

with J_{ij} the synaptic coupling from neuron j to neuron i . In the sequel we write the shorthand notation $h_{N,i}(t) \equiv h_i(\boldsymbol{\sigma}_N(t))$.

It is clear that the J_{ij} explicitly depend on the architecture. For the extremely diluted (ED), both symmetric (SED) and asymmetric (AED), and the fully connected (FC) architectures the couplings are time-independent and the diagonal terms are absent, i.e. $J_{ii} = 0$. The configuration $\boldsymbol{\sigma}_N(t = 0)$ is chosen as input. For the layered feedforward (LF) model the time dependence of the couplings is relevant because the set-up of the model is somewhat different. There, each neuron in layer t is unidirectionally connected to all neurons on layer $t + 1$ and $J_{ij}(t)$ is the strength of the coupling from neuron j on layer t to neuron i on layer $t + 1$. The state $\boldsymbol{\sigma}_N(t + 1)$ of layer $t + 1$ is determined by the state $\boldsymbol{\sigma}_N(t)$ of the previous layer t .

In all cases the couplings are chosen according to the Hebb rule such that we can write

$$J_{ij}^{ED} = \frac{c_{ij}}{CA} \sum_{\mu=1}^p \xi_i^\mu \xi_j^\mu \quad \text{for } i \neq j, \quad (2)$$

$$J_{ij}^{FC} = \frac{1}{NA} \sum_{\mu=1}^p \xi_i^\mu \xi_j^\mu \quad \text{for } i \neq j, \quad (3)$$

$$J_{ij}^{LF}(t) = \frac{1}{NA} \sum_{\mu=1}^p \xi_i^\mu(t+1) \xi_j^\mu(t), \quad (4)$$

with the $\{c_{ij} = 0, 1\}, i, j = 1, \dots, N$ chosen to be i.i.d.r.v. with distribution $\Pr\{c_{ij} = x\} = (1 - C/N)\delta_{x,0} + (C/N)\delta_{x,1}$ and satisfying for symmetric dilution $c_{ij} = c_{ji}$, $c_{ii} = 0$, and for asymmetric dilution that c_{ij} and c_{ji} are statistically independent (with $c_{ii} = 0$).

All neurons are updated in parallel through the spin-flip dynamics defined by the transition probabilities

$$\Pr\{\sigma_i(t+1) = s_k \in \mathcal{S} | \boldsymbol{\sigma}_N(t)\} = \frac{\exp[-\beta \epsilon_i(s_k | \boldsymbol{\sigma}_N(t))]}{\sum_{s \in \mathcal{S}} \exp[-\beta \epsilon_i(s | \boldsymbol{\sigma}_N(t))]} \cdot \quad (5)$$

Here the energy potential $\epsilon_i[s | \boldsymbol{\sigma}_N]$ is defined by [69]

$$\epsilon_i[s | \boldsymbol{\sigma}_N] = -\frac{1}{2} [h_i(\boldsymbol{\sigma}_N) s - b s^2], \quad (6)$$

where $b > 0$ is the gain parameter of the system. The zero temperature limit $T = \beta^{-1} \rightarrow 0$ of this dynamics is given by the updating rule

$$\sigma_i(t) \rightarrow \sigma_i(t+1) = s_k : \min_{s \in \mathcal{S}} \epsilon_i[s | \boldsymbol{\sigma}_N(t)] = \epsilon_i[s_k | \boldsymbol{\sigma}_N(t)]. \quad (7)$$

This updating rule (7) is equivalent to using a gain function $\mathbf{g}_b(\cdot)$,

$$\begin{aligned} \sigma_i(t+1) &= \mathbf{g}_b(h_{N,i}(t)) \\ \mathbf{g}_b(x) &\equiv \sum_{k=1}^Q s_k [\theta [b(s_{k+1} + s_k) - x] - \theta [b(s_k + s_{k-1}) - x]] \end{aligned} \quad (8)$$

with $s_0 \equiv -\infty$ and $s_{Q+1} \equiv +\infty$. For finite Q , this gain function $\mathbf{g}_b(\cdot)$ is a step function. The gain parameter b controls the average slope of $\mathbf{g}_b(\cdot)$.

In order to measure the retrieval quality of the system one can use the Hamming distance between a stored pattern and the microscopic state of the network

$$d(\boldsymbol{\xi}^\mu, \boldsymbol{\sigma}_N(t)) \equiv \frac{1}{N} \sum_i [\xi_i^\mu - \sigma_i(t)]^2. \quad (9)$$

This introduces the main overlap and the arithmetic mean of the neuron activities

$$m_N^\mu(t) = \frac{1}{NA} \sum_i \xi_i^\mu \sigma_i(t), \quad \mu = 1, \dots, p; \quad a_N(t) = \frac{1}{N} \sum_i [\sigma_i(t)]^2. \quad (10)$$

We remark that for $Q = 2$ the variance of the patterns $A = 1$, and the neuron activity $a(t) = 1$. For the LF architecture we recall that ξ_i^t depends on t .

In this overview we mainly consider the patterns to be uniformly distributed (e.g., $A = 2/3$ for $Q = 3$). For low-activity networks (A small, e.g., $A \ll 2/3$ for $Q = 3$) a better measure for the retrieval quality is the mutual information. We refer to the literature for a further discussion of this point [81]–[83] (and references therein).

2.2 Solving the dynamics

2.2.1 Correlations

We first discuss some of the geometric properties of the various architectures which are particularly relevant for the understanding of their long-time dynamic behaviour.

For a FC architecture there are two main sources of strong correlations between the neurons complicating the dynamical evolution : feedback loops and the common ancestor problem [18]. Feedback loops occur when in the course of the time evolution, e.g., the following string of connections is possible: $i \rightarrow j \rightarrow k \rightarrow i$. We remark that architectures with symmetric connections always have these feedback loops. In the absence of these loops the network functions in fact as a layered system, i.e., only feedforward connections are possible. But in this layered architecture common ancestors are still present when, e.g., for the sites i and j there are sites in the foregoing time steps that have a connection with both i and j .

In AED architectures these sources of correlations are absent. This class of neural networks was introduced in connection with $Q = 2$ -Ising models [42]. We recall that the couplings are then given by eq. (2) and that in the limit $N \rightarrow \infty$ two important properties of this network are essential [42], [84]. The first property is the high asymmetry of the connections, viz.

$$\Pr\{c_{ij} = c_{ji}\} = \left(\frac{C}{N}\right)^2, \quad \Pr\{c_{ij} = 1 \wedge c_{ji} = 0\} = \frac{C}{N} \left(1 - \frac{C}{N}\right). \quad (11)$$

Therefore, almost all connections of the graph $G_N(\mathbf{c}) = \{(i, j) : c_{ij} = 1, i, j \neq i = 1, \dots, N\}$ are directed : $c_{ij} \neq c_{ji}$. The second property in the limit of extreme dilution is the directed local Cayley-tree structure of the graph $G_N(\mathbf{c})$. By the arguments above the probability that k connections are directed towards a given site i becomes a Poisson distribution in the limit of extreme dilution and the mean value of the number of in(out) connections for this site i is C . The probability that the sites i and i' have site j as a common ancestor is obviously C/N , hence the probability that the sites i and i' have disjoint clusters of ancestors approaches $(1 - C^t/N)^{C^t} \simeq \exp(-C^{2t}/N)$ for $N \gg 1$.

So we find that in the limit of extreme dilution almost all (i.e. with probability 1) feedback loops are eliminated. and any finite number of neurons have almost all disjoint clusters of ancestors. So we first dilute the system by taking $N \rightarrow \infty$ and then we take the limit $C \rightarrow \infty$ in order to get infinite average connectivity allowing to store infinitely many patterns p .

This implies that for this AED model at any given time step t all spins are uncorrelated and, hence, the first step dynamics describes the full time evolution of the network.

For the SED model the architecture is still a local Cayley-tree but no longer directed and in the limit $N \rightarrow \infty$ the probability that the number of connections giving information to the the site i , is still a Poisson distribution with mean C . However, at time t the spins are no longer uncorrelated causing a feedback from $t \geq 2$ onwards [61], [62].

2.2.2 First time step

In order to solve the dynamics we start with a discussion of the first time step dynamics, the form of which is independent of the architecture. So consider a FC network. Suppose that the initial configuration of the network $\{\sigma_i(0)\}$ is a collection of i.i.d.r.v. with mean $E[\sigma_i(0)] = 0$, variance $\text{Var}[\sigma_i(0)] = a_0$, and correlated with only one stored pattern, say the first one $\{\xi_i^1\}$:

$$E[\xi_i^\mu \sigma_j(0)] = \delta_{i,j} \delta_{\mu,1} m_0^1 A \quad m_0^1 > 0. \quad (12)$$

This pattern is said to be condensed. By the law of large numbers (LLN) one gets for the main overlap and the activity at $t = 0$

$$m^1(0) \equiv \lim_{N \rightarrow \infty} m_N^1(0) \stackrel{Pr}{=} \frac{1}{A} E[\xi_i^1 \sigma_i(0)] = m_0^1 \quad (13)$$

$$a(0) \equiv \lim_{N \rightarrow \infty} a_N(0) \stackrel{Pr}{=} E[\sigma_i^2(0)] = a_0 \quad (14)$$

where the convergence is in probability (e.g., [85]). In order to obtain the configuration at $t = 1$ we first have to calculate the local field (1) at $t = 0$. To do this we employ the signal-to-noise ratio analysis (see, e.g., [40], [45]). Recalling the learning rule (3) we separate the part containing the condensed pattern, i.e., the signal, from the rest, i.e., the noise to arrive at

$$h_i(\boldsymbol{\sigma}_N(0)) = \xi_i^1 \frac{1}{NA} \sum_{j \neq i} \xi_j^1 \sigma_j(0) + \sqrt{\alpha} \frac{1}{\sqrt{pA}} \sum_{\mu \neq 1} \xi_i^\mu \frac{1}{\sqrt{NA}} \sum_{j \neq i} \xi_j^\mu \sigma_j(0) \quad (15)$$

where $\alpha = p/N$. The properties of the initial configurations (12)-(14) assure us that the summation in the first term on the r.h.s of (15) converges in the limit

$N \rightarrow \infty$ to

$$\lim_{N \rightarrow \infty} \frac{1}{NA} \sum_{j \neq i} \xi_j^1 \sigma_j(0) \stackrel{Pr}{=} m^1(0). \quad (16)$$

The first term $\xi_i^1 m^1(0)$ is independent of the second term on the r.h.s of (15). This second term contains the influence of the non-condensed patterns causing the intrinsic noise in the dynamics of the main overlap. In view of this we define the residual overlap

$$r^\mu(t) \equiv \lim_{N \rightarrow \infty} r_N^\mu(t) = \lim_{N \rightarrow \infty} \frac{1}{A\sqrt{N}} \sum_j \xi_j^\mu \sigma_j(t) \quad \mu \neq 1. \quad (17)$$

Applying the CLT to this second term in (15) we find

$$\lim_{N \rightarrow \infty} \sqrt{\frac{\alpha}{p}} \sum_{\mu \neq 1} \xi_i^\mu r_{N \setminus i}^\mu(0) = \lim_{N \rightarrow \infty} \sqrt{\alpha} \frac{1}{\sqrt{p}} \sum_{\mu \neq 1} \xi_i^\mu \frac{1}{A\sqrt{N}} \sum_{j \neq i} \xi_j^\mu \sigma_j(0) \quad (18)$$

$$\stackrel{D}{=} \sqrt{\alpha} \mathcal{N}(0, AD(0)) \quad (19)$$

where the quantity $\mathcal{N}(0, V)$ represents a Gaussian random variable with mean 0 and variance V and where $D(0) = \text{Var}[r^\mu(0)] = a(0)$. Thus we see that in fact the variance of this residual overlap, i.e., $D(t)$ is the relevant quantity characterising the intrinsic noise.

In conclusion, in the limit $N \rightarrow \infty$ the local field is the sum of two independent random variables, i.e.

$$h_i(0) \equiv \lim_{N \rightarrow \infty} h_{N,i}(0) \stackrel{D}{=} \xi_i^1 m^1(0) + \sqrt{\alpha} \mathcal{N}(0, a(0)). \quad (20)$$

At this point we note that the structure (20) of the distribution of the local field at time zero – signal plus Gaussian noise – is typical for all architectures discussed here because the correlations caused by the dynamics only appear for $t \geq 1$. Some technical details are different for the various architectures. The first change in details that has to be made is an adaptation of the sum over the sites j to all i for the LF architecture and to the part of the tree connected to neuron i which has mean C , in the ED architectures. The second change is that for the diluted architectures an additional limit $C \rightarrow \infty$ has to be taken besides the $N \rightarrow \infty$ limit. So in the thermodynamic limit $C, N \rightarrow \infty$ all averages will have to be taken over the treelike structure, viz. $\frac{1}{N} \sum_i \rightarrow \frac{1}{C} \sum_{i \in \text{tree}}$. Furthermore $\alpha = p/N$ has to be replaced by $\alpha = p/C$.

2.2.3 Recursive dynamical scheme

The key question is then how these quantities evolve in time under the parallel dynamics specified before. For a general time step we find from the LLN in the limit $C, N \rightarrow \infty$ for the main overlap and the activity (10)

$$m^1(t+1) \stackrel{Pr}{=} \frac{1}{A} \langle \langle \xi_i^1 \langle \sigma_i(t+1) \rangle_\beta \rangle \rangle, \quad a(t+1) \stackrel{Pr}{=} \langle \langle \sigma_i(t+1) \rangle_\beta^2 \rangle \quad (21)$$

with the thermal average defined as

$$\langle f(\sigma_i(t+1)) \rangle_\beta = \frac{\sum_{\sigma \in \mathcal{S}} f(\sigma) \exp[\frac{1}{2}\beta \sigma (h_i(t) - b\sigma)]}{\sum_{\sigma \in \mathcal{S}} \exp[\frac{1}{2}\beta \sigma (h_i(t) - b\sigma)]} \quad (22)$$

where $h_i(t) \equiv \lim_{N \rightarrow \infty} h_{N,i}(t)$. In the above $\langle \langle \cdot \rangle \rangle$ denotes the average both over the distribution of the embedded patterns $\{\xi_i^\mu\}$ and the initial configurations $\{\sigma_i(0)\}$. The average over the latter is hidden in an average over the local field through the updating rule (8). In the sequel we focus on zero temperature. Then, using eq. (8) these formula reduce to

$$m^1(t+1) \stackrel{Pr}{=} \frac{1}{A} \langle \langle \xi_i^1 \mathbf{g}_b(h_i(t)) \rangle \rangle, \quad a(t+1) \stackrel{Pr}{=} \langle \langle \mathbf{g}_b^2(h_i(t)) \rangle \rangle. \quad (23)$$

As seen already in the first time step, we have to study carefully the influence of the non-condensed patterns causing the intrinsic noise in the dynamics of the main overlap. The method used to obtain these order parameters is then to calculate the distribution of the local field as a function of time. In order to determine the structure of the local field we have to concentrate on the evolution of the residual overlap. The details of this calculation are very technical and depend on the precise correlations in the system and hence on the architecture of the network [2], [3], [45], [53], [60]. Here we give a discussion of the results obtained.

In general, the distribution of the local field at time $t+1$ is given by

$$h_i(t+1) = \xi_i^1 m^1(t+1) + \mathcal{N}(0, \alpha a(t+1)) + \chi(t) [F(h_i(t) - \xi_i^1 m^1(t)) + B \alpha \sigma_i(t)] \quad (24)$$

where F and B are binary coefficients given below, which depend on the specific architecture. From this it is clear that the local field at time t consists out of a discrete part and a normally distributed part, viz.

$$h_i(t) = M_i(t) + \mathcal{N}(0, V(t)) \quad (25)$$

where $M_i(t)$ satisfies the recursion relation

$$M_i(t+1) = \chi(t) [F(M_i(t) - \xi_i^1 m^1(t)) + B \alpha \sigma_i(t)] + \xi_i^1 m^1(t+1) \quad (26)$$

and where $V(t) = \alpha AD(t)$ with $D(t)$ itself given by the recursion relation

$$D(t+1) = \frac{a(t+1)}{A} + L\chi^2(t)D(t) + 2B_2\chi(t)\text{Cov}[\tilde{r}^\mu(t), r^\mu(t)] \quad (27)$$

where L and B_2 are again coefficients specified below. The quantity $\chi(t)$ reads

$$\chi(t) = \sum_{k=1}^{Q-1} f_{\hat{h}_i^\mu(t)}(b(s_{k+1} + s_k))(s_{k+1} - s_k) \quad (28)$$

where $f_{\hat{h}_i^\mu(t)}$ is the probability density of $\hat{h}_i^\mu(t) = \lim_{N \rightarrow \infty} \hat{h}_{N,i}^\mu(t)$ with

$$\hat{h}_{N,i}^\mu(t) = h_{N,i}(t) - \frac{1}{\sqrt{N}} \xi_i^\mu r_{N,i}^\mu(t). \quad (29)$$

Furthermore, $\tilde{r}^\mu(t)$ is defined as

$$\tilde{r}^\mu(t) \equiv \lim_{N \rightarrow \infty} \frac{1}{A\sqrt{N}} \sum_i \xi_i^\mu \mathbf{g}_b(\hat{h}_{N,i}^\mu(t)). \quad (30)$$

At this point we remark that we made the technical assumption that $\sigma_i(t)$ and $\hat{h}_{N,i}^\mu(t)$ are only weakly correlated in the limit $N \rightarrow \infty$ such that $\tilde{r}^\mu(t)$ converges to a normal distribution. Finally, as can be read off from eq. (26) the quantity $M_i(t)$ consists out of the signal term and a discrete noise term, viz.

$$M_i(t) = \xi_i^1 m^1(t) + B_1 \alpha \chi(t-1) \sigma_i(t-1) + B_2 \sum_{t'=0}^{t-2} \alpha \left[\prod_{s=t'}^{t-1} \chi(s) \right] \sigma_i(t'). \quad (31)$$

Since different architectures contain different correlations not all terms in these final equations are present. In particular we have for the coefficients F, B, L, B_1 and B_2 introduced above

	F	B	L	B_1	B_2
FC	1	1	1	1	1
SED	0	1	0	1	0
LF	1	0	1	0	0
AED	0	0	0	0	0

(32)

with B indicating the feedback caused by the symmetry in the architectures and L the common ancestors contribution.

At this point we remark that in the so-called theory of statistical neurodynamics [28], [35], [81] one starts from a different approximate local field by leaving out

any discrete noise (the term in $\sigma_i(t)$). As a consequence the covariance in the recursion relation for $D(t)$ can be written down more explicitly since only Gaussian noise is involved. For more details we refer to [28], [67], [86].

We still have to determine the probability density of $f_{h_i^\mu(t)}$ in eq. (28), which in the thermodynamic limit equals the probability density of $f_{h_i(t)}$. This can be done by looking at the form of $M_i(t)$ given by eq. (31). The evolution equation tells us that $\sigma_i(t')$ can be replaced by $g_b(h_i(t' - 1))$ such that the second and third terms of $M_i(t)$ are the sums of stepfunctions of correlated variables. These are also correlated through the dynamics with the normally distributed part of $h_i(t)$. Therefore the local field can be considered as a transformation of a set of correlated normally distributed variables x_s , $s = 0, \dots, t-2, t$, which we choose to normalize. Defining the correlation matrix $W = (\rho(s, s') \equiv E[x_s x_{s'}])$ we arrive at the following expression for the probability density of the local field at time t

$$f_{h_i(t)}(y) = \int \prod_{s=0}^{t-2} dx_s dx_t \delta\left(y - M_i(t) - \sqrt{\alpha AD(t)} x_t\right) \times \frac{1}{\sqrt{\det(2\pi W)}} \exp\left(-\frac{1}{2} \mathbf{x} W^{-1} \mathbf{x}^T\right) \quad (33)$$

with $\mathbf{x} = (x_0, \dots, x_{t-2}, x_t)$. For the symmetrically diluted case this expression simplifies to

$$f_{h_i(t)}(y) = \int \prod_{s=0}^{[t/2]} dx_{t-2s} \delta\left(y - \xi_i^1 m^1(t) - \alpha \chi(t) \sigma_i(t) - \sqrt{\alpha a(t)} x_t\right) \times \frac{1}{\sqrt{\det(2\pi W)}} \exp\left(-\frac{1}{2} \mathbf{x} W^{-1} \mathbf{x}^T\right) \quad (34)$$

with $\mathbf{x} = (\{x_s\}) = (x_{t-2[t/2]}, \dots, x_{t-2}, x_t)$. The brackets $[t/2]$ denote the integer part of $t/2$.

So the local field at time t consists out of a signal term, a discrete noise part and a normally distributed noise part. Furthermore, the discrete noise and the normally distributed noise are correlated and this prohibits us to derive a closed expression for the overlap and activity.

Together with the eqs. (23) for $m^1(t+1)$ and $a(t+1)$ the results above form a recursive scheme in order to obtain the order parameters of the system. The practical difficulty which remains is the explicit calculation of the correlations in the network at different time steps as present in eq. (27).

For AED and LF architectures this scheme leads to an explicit form for the recursion relations for the order parameters

$$m^\mu(t+1) = \frac{\delta_{\mu,1}}{A} \left\langle \left\langle \xi^1(t+1) \int \mathcal{D}z g_b(\xi^1(t+1)m^1(t) + \sqrt{\alpha AD(t)} z) \right\rangle \right\rangle \quad (35)$$

$$a(t+1) = \left\langle\left\langle \int \mathcal{D}z g_b^2(\xi^1(t+1)m^1(t) + \sqrt{\alpha AD(t)} z) \right\rangle\right\rangle \quad (36)$$

$$D(t+1) = \frac{a(t+1)}{A} + \frac{L}{\alpha A} \left\langle\left\langle \int \mathcal{D}z z g_b(\xi^1(t+1)m^1(t) + \sqrt{\alpha AD(t)} z) \right\rangle\right\rangle^2 \quad (37)$$

with $\mathcal{D}z = dz(2\pi)^{-1/2} \exp(-z^2/2)$. For the AED architecture ($L = 0$) the second term on the r.h.s. of (37) coming from the correlations caused by the common ancestors is absent. For the LF architecture we remark that this explicit solution requires an independent choice of the representations of the patterns at different layers.

At finite temperatures analogous recursion relations for the AED and LF networks can be derived [45], [53] by introducing auxiliary thermal fields [87] in order to express the stochastic dynamics within the gain function formulation of the deterministic dynamics. These recursion relations can be solved numerically and the stationary limit can be discussed (see Section 2.2.4). Furthermore, damage spreading [42], [88], [89], i.e., the evolution of two network configurations which are initially close in Hamming distance can be studied [45], [53]. Finally, a complete self-control mechanism can be built in the dynamics of these systems by introducing a time-dependent threshold in the gain function improving, e.g., the storage capacity, the basins of attraction of the embedded patterns and the mutual information content [81]–[83], [90]

For the symmetric networks explicit examples of the dynamical scheme above and a comparison with numerical simulations have been presented in [2] for the FC and in [60] for the SED model with equidistant states and a uniform distribution of the patterns. By using the recursion relations the first few time steps are written out explicitly and studied numerically. These results are compared with the literature [34], [35], [40], [41], [61], [62], [81], [91]–[95] where the feedback correlations for $t \geq 2$ are neglected or approximated in different ways. In the whole retrieval region of these symmetric networks it is found that the first four or five time steps calculated by the scheme presented above give already a clear picture of the time evolution. Explicit results depend of course on the specific values of the model parameters, e.g., the storage capacity α , the initial overlap m_0 with the embedded pattern, the initial neural activity a_0 , the value of the gain parameter b . Furthermore, numerical simulations provide good support for this scheme, but very recently we have discovered some small deviations, especially close to the border of retrieval which can not be entirely due to finite size effects. This has been completely understood recently by carefully studying the long time correlations and the details are being worked out (see [67], [96] and Section 3.2).

2.2.4 Stationary limit: thermodynamic and retrieval properties

Equilibrium results for the AED and LF Q -Ising models are obtained immediately by straightforwardly leaving out the time dependence in (35)-(37) (cfr. [45],[53]), since the evolution equations for the local field and the order parameters do not change their form as time progresses. This still allows small fluctuations in the configurations $\{\sigma_i\}$. The difference between the fixed-point equations for these two architectures is that for the AED model the variance of the residual noise, $D(t)$, is simply proportional to the activity of the neurons at time t while for the LF model a recursion is needed.

A lot of detailed results are available on capacity-gain parameter and temperature capacity diagrams obtained by numerically solving these equations. In general, it is necessary to distinguish three different types of solutions. The zero solution, Z , is determined by $m = 0$ as well as $a = 0$. A sustained activity solution, S , is defined by $m = 0$ but $a \neq 0$. Finally, there are solutions with both $m \neq 0$ and $a \neq 0$. Nonattracting solutions of the last type are denoted by NR (for non-retrieval), attracting ones by R (for retrieval). As a typical illustration we show fig. 1.

For the AED architecture it is important to observe that, for zero temperature, in the retrieval regime, R is never the only attractor in the (m, a) plane. Its basin of attraction is always limited by at least one attractor on the axis $m = 0$. In contrast, in the case of analog neurons (piecewise linear networks) the retrieval solution is an attractor for the whole (m, a) plane. Furthermore, at any fixed α , a value of b can be determined where the Hamming distance of R is minimal. The line of these optimal b is indicated by OPT . It is close to $1/2$ for $T = 0$ and shifts completely to $b = 0$ with increasing temperature. Finally, for a finite Q network two arbitrarily close configurations always repel each other even in the retrieval regime. For analog networks there exists a transition line in the capacity-gain plane below which no such “chaotic” behaviour occurs.

For the LF architecture at zero temperature, in contrast to the AED case, the retrieval state is always accompanied by an attractor which has zero overlap with the embedded pattern. In all cases under consideration the retrieval state disappears discontinuously as the storage capacity α increases. Finally, a type of chaoticity in the network trajectories is always present for arbitrary finite Q . However, in the case of a piecewise linear gain function there exists a dynamical transition towards chaos in the (α, b) -plane. The (α, b) -region where chaos does occur is relatively smaller than in the corresponding AED networks. For further results and especially for results at finite temperature, we refer to the literature mentioned before.

Next, for the SED and FC architectures the evolution equations for the order parameters do change their form as time progresses by the explicit appearance of

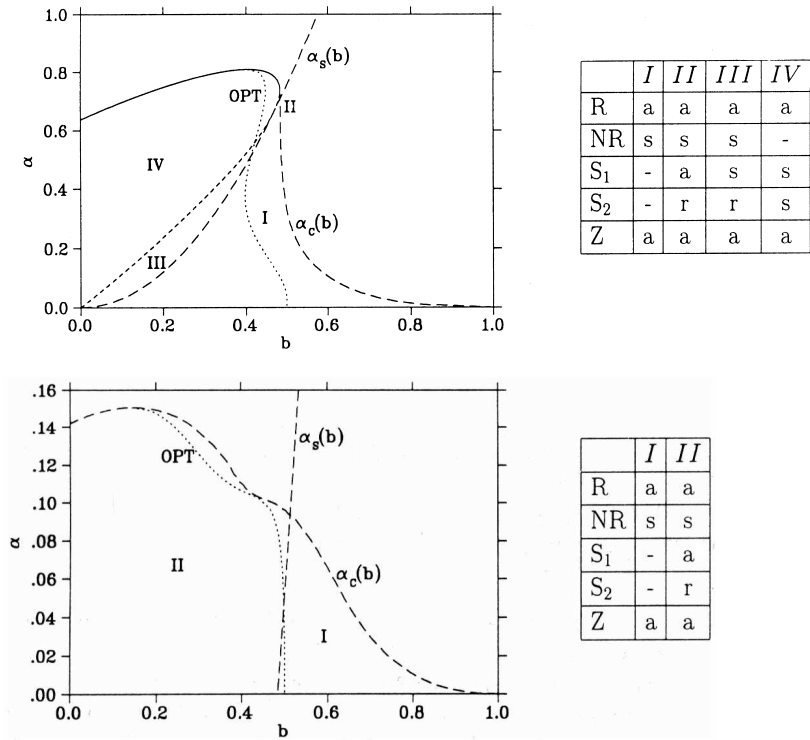


Figure 1: The $(\alpha - b)$ diagram for the $Q = 3$ AED (top) and LF (bottom) network with uniform patterns at $T = 0$. The curve $\alpha_c(b)$ denotes the boundary of the retrieval region. The curve $\alpha_s(b)$ is the lower bound for the existence of the sustained activity states. The full line denotes a second-order transition, the dashed line a first order one. The line OPT is the line of best retrieval quality. The structure of the retrieval dynamics is explained: a denotes an attractor, s a saddle-point, r a repellor.

the $\{\sigma_i(t')\}$, $t' = 1, \dots, t$ term. Hence we can not use the simple procedure above to obtain the fixed-point equations. Instead we derive the equilibrium results of our dynamical scheme by requiring through the recursion relations (24) that the distribution of the local field becomes time-independent. This is clearly an approximation because fluctuations in the network configuration are no longer allowed. In fact, it means that out of the discrete part of this distribution, i.e., $M_i(t)$ (recall (31)), only the $\sigma_i(t-1)$ term is kept besides, of course, the signal term. This procedure implies that the main overlap and activity in the fixed-point are found from the definitions (10) and not from leaving out the time dependence in the recursion relation (23).

We start by eliminating the time-dependence in the evolution equations for the local field (24). This leads to

$$h_i = \xi_i^1 m^1 + [\bar{\chi}^{ar}]^{-1} \mathcal{N}(0, \alpha a) + [\bar{\chi}^{ar}]^{-1} \alpha \chi \sigma_i \quad (38)$$

with $\bar{\chi}^{ar} \equiv 1 - F\chi$ being 1 for the SED and $1 - \chi$ for the FC model and $h_i \equiv \lim_{t \rightarrow \infty} h_i(t)$. This expression consists out of two parts: a normally distributed part $\tilde{h}_i = \mathcal{N}(\xi_i^1 m^1, \alpha a / [\bar{\chi}^{ar}]^2)$ and some discrete noise part. The discrete noise comes from the correlations of the $\{\sigma_i(t)\}$ at different time steps (here only the preceding time step is considered) and is inherent in the SED and FC dynamics. Employing this expression in the updating rule (8) one finds

$$\sigma_i = \mathbf{g}_b(\tilde{h}_i + [\bar{\chi}^{ar}]^{-1} \alpha \chi \sigma_i). \quad (39)$$

This is a self-consistent equation in σ_i which in general admits more than one solution. These types of equation have been solved in the literature in the context of thermodynamics using a geometric Maxwell construction [39], [97]. We remark that for analog networks the geometric Maxwell construction is not necessary: the fixed-point equation (39) has only one solution [86].

This approach leads to a unique solution

$$\sigma_i = \mathbf{g}_{\tilde{b}}(\tilde{h}_i), \quad \tilde{b} = b - [2\bar{\chi}^{ar}]^{-1} \alpha \chi. \quad (40)$$

We remark that plugging this result into the local field (38) tells us that the probability distribution of the local field contains $(Q-1)$ gaps. This gap structure also depends on the architecture and the most important findings are that dilution changes the regions of existence of these gaps but not their width. Moreover, the gaps become typically much bigger when crossing the border of retrieval [98]–[100].

Using the definition of the main overlap and activity (10) in the limit $N \rightarrow \infty$ for the FC model and limit $C, N \rightarrow \infty$ for the SED model, one finds in the fixed

point

$$m^1 = \left\langle\left\langle \xi^1 \int \mathcal{D}z \mathbf{g}_{\tilde{b}} \left(\xi^1 m^1 + \sqrt{\alpha AD} z \right) \right\rangle\right\rangle \quad (41)$$

$$a = \left\langle\left\langle \int \mathcal{D}z \mathbf{g}_{\tilde{b}}^2 \left(\xi^1 m^1 + \sqrt{\alpha AD} z \right) \right\rangle\right\rangle. \quad (42)$$

From (27) and (28) one furthermore sees that

$$D = [\bar{\chi}^{ar}]^{-2} a/A \quad (43)$$

with

$$\chi = \frac{1}{\sqrt{\alpha AD}} \left\langle\left\langle \int \mathcal{D}z z \mathbf{g}_{\tilde{b}} \left(\xi^1 m^1 + \sqrt{\alpha AD} z \right) \right\rangle\right\rangle. \quad (44)$$

These resulting equations (41)-(43) obtained through *parallel* dynamics turn out to be the same as the fixed-point equations derived from a replica-symmetric mean-field theory treatment discussed next.

For symmetric networks (FC and SED) we consider the long time behaviour governed by the Hamiltonian

$$H^{ar} = -\frac{1}{2} \sum_{i \neq j} J_{ij}^{ar} \sigma_i \sigma_j + b \sum_i \sigma_i^2. \quad (45)$$

with $J_{i,j}^{ar}$ given by (3) for the FC and by (2) for the SED model. The neurons are updated *asynchronously* according to the transition probability (5)-(6). In order to calculate the free energy we use the standard replica method [11], [68]. We remark that for the SED architecture, we employ the replica method as applied to dilute spin-glass models [101]–[104]. Starting from the replicated partition function averaged over the connectivity and the non-condensed patterns and assuming replica symmetry, we arrive at the free energy $f(\beta)$ which can be written down for a variable dilution $c = C/N$ with c between 0 (SED) and 1 (FC)

$$f(\beta) = \frac{A}{2} \sum_{\mu=1}^s (m_{\mu})^2 + \frac{\alpha c}{2\beta} \left[\ln(1 - \chi) + \frac{\chi}{1 - \chi} + \frac{q\beta\chi}{(1 - \chi)^2} \right] - \frac{1}{\beta} \left\langle\left\langle \int \mathcal{D}z \ln \text{Tr}_{\{\sigma\}} \exp \left[\beta \sigma \left(\sum_{\mu} m_{\mu} \xi^{\mu} + z \sqrt{\alpha rc} - \tilde{b} \sigma \right) \right] \right\rangle\right\rangle_{\{\xi\}} \quad (46)$$

with s the number of condensed patterns which we take to be 1 as before,

$$\tilde{b} = b - \frac{\alpha\chi}{2} \left[1 + \frac{c\chi}{1 - \chi} \right], \quad r = q \left[\frac{1}{(1 - \chi)^2} + \frac{1 - c}{c} \right] \quad (47)$$

with q the Edwards-Anderson spin-glass order parameter and $\chi = \beta \langle\langle \sigma^2 \rangle - \langle \sigma \rangle^2 \rangle$ the susceptibility (defined before in Section 2.2.3 for zero temperature) in the stationary limit. We remark that the effective gain parameter \tilde{b} can be negative, implying that the input-output function reduces to that of 2-Ising-type neurons, i.e., $g_{\tilde{b}}(h) = \text{sign}(h)$.

The phase structure of the network is determined by the solution of the fixed-point equations for the order parameters

$$m_\mu = \frac{1}{A} \langle\langle \int Dz \xi^\mu \langle \sigma(z) \rangle \rangle \rangle \quad (48)$$

$$q = \langle\langle \int Dz \langle \sigma(z)^2 \rangle \rangle \rangle \quad (49)$$

$$\chi = \frac{1}{\sqrt{\alpha rc}} \langle\langle \int Dz z \langle \sigma(z) \rangle \rangle \rangle \quad (50)$$

which maximize $-\beta f(\beta)$. Here

$$\langle \sigma(z) \rangle = \frac{\text{Tr}_{\sigma} \sigma \exp[\beta \sigma (\sum_{\mu} m_{\mu} \xi^{\mu} + z \sqrt{\alpha rc} - \tilde{b} \sigma)]}{\text{Tr}_{\sigma} \exp[\beta \sigma (\sum_{\mu} m_{\mu} \xi^{\mu} + z \sqrt{\alpha rc} - \tilde{b} \sigma)]}. \quad (51)$$

Explicit expressions for these fixed-point equations for $Q = 3, 4$ and $Q = \infty$ can be found in [69], [70], [73] for the FC and SED model and for $Q = 3$ in [63] for variable dilution.

A lot of detailed results are available on the corresponding phase diagrams. Some typical results are shown in fig. 2. In general, we can distinguish a retrieval phase ($m \neq 0$), a spin-glass phase ($m = 0, q > 0$) and a paramagnetic phase ($m = 0, q = 0$). For the FC architecture at zero temperature the results are extremely dependent on the pattern activity. In the case of uniformly distributed patterns ($A = 2/3$) we see that different retrieval regions show up for small b (the retrieval region II does not appear for $A < 1/3$) and the capacity is reduced by a factor compared with the capacity for the AED and LF architectures. The line of optimal Hamming distance is given exactly by $b = 1/2$ (fig 2 left); in the AED model we recall that it is located for the whole retrieval region in the interval $b \in [0.4, 0.5]$ (see fig. 1 top) while in the LF model it bends to smaller b for growing a (see fig. 1 bottom). We remark that for $Q = \infty$ the diagram for the FC and LF models are very similar in shape but the capacity is reduced roughly by a factor of 10 in the former. For non-zero temperatures the situation is complicated and depends very much on the value of b . For b close to and greater than the optimal $b = 1/2$ the phase diagram is completely different from that of the Hopfield model in the sense that the paramagnetic phase exists between the retrieval and the spin-glass phase

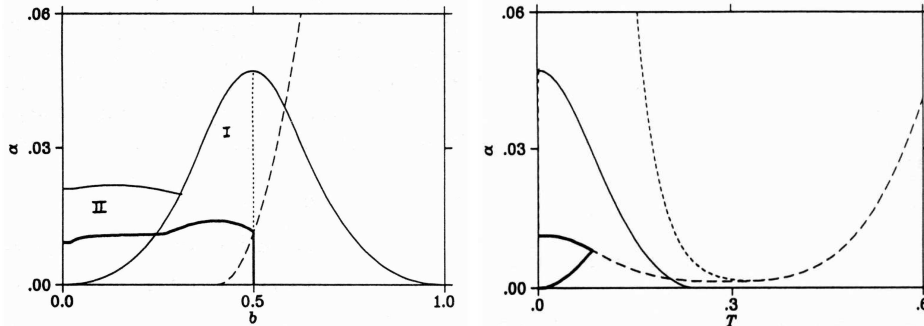


Figure 2: The $(\alpha - b)$, $T = 0$ (left) and $(\alpha - T)$, $b = \frac{1}{2}$ (right) phase diagram for the FC $Q = 3$ -Ising model with uniform patterns. The (thin) full curve represents the boundary of the retrieval region, the thick full curve the thermodynamic transition of the retrieval state, the long-dashed curve the spin-glass transition, and the dotted curve the optimal gain parameter. The I and II indicate two retrieval regions: in region I $r \approx O(1)$, while in region II $r \approx O(10)$. The chain curve (very close to the α -axis on the right) is the AT-line. The short dashed curve indicates the border above which no paramagnetic states exists.

(see fig. 2 right). We remark that for $Q = \infty$ the diagram is relatively simple again and qualitatively resembles that of the Hopfield model.

For the SED architecture there are interesting similarities with the AED model. In fact, we find that the $(\alpha - b)$ phase diagram in fig. 3 is tilted towards higher b -values in comparison with fig. 1 (top) because of the presence of an extended 2-Ising-like region. The critical boundary of this region is independent of Q . The $(\alpha - T)$ diagram of the $Q = 3$ and $Q = \infty$ models are qualitatively similar.

For variable dilution (all values of $c \in [0, 1]$) one finds some architecture independent properties for $\alpha \rightarrow 0$, e.g., the optimal value of b being $b = 1/2$ for $T = 0$. The main dependence of the behaviour of the network on the connectivity arises for finite α . An interesting property is the suppression of the discontinuous boundary between the retrieval regions I and II (see fig. 2 left) with decreasing connectivity, disappearing completely for $c \approx 0.63$, making the optimal performance domain readily accessible to a wide region of network parameters [63].

Finally, the stability of the replica symmetric retrieval solution against replica-symmetry breaking can be determined by studying the replicon eigenvalue [68] [105], leading to the de Almeida-Thouless (AT) stability line indicating the temperatures below which the replica-symmetric approximation is no longer valid. For more details we refer to the figures shown and to the literature mentioned before.

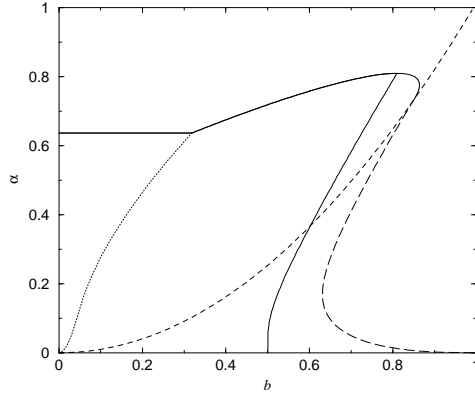


Figure 3: The $(\alpha - b)$ phase diagram for the $Q = 3$ SED model with uniform patterns at $T = 0$. The (thin) full and long-dashed curves denote the boundary of the retrieval region corresponding respectively to a continuous and discontinuous appearance of the solution. The dotted curve separates the 2-Ising-like retrieval region. The short-dashed curve indicates the discontinuous spin-glass transition. The thick full curve represents the thermodynamic transition for the retrieval state.

3 BEG neural networks

3.1 The model

In Section 2.1 it has been mentioned that the mutual information [106], [107] is the most appropriate concept to measure the retrieval quality for sparsely coded networks. A natural question is then whether one could use the mutual information in general in a systematic way to determine a priori an optimal hamiltonian guaranteeing the best retrieval properties including, e.g., the largest retrieval overlap, loading capacity, basin of attraction, convergence time, for an arbitrary scalar valued neuron (spin) model. Optimal means especially that although the network might start initially *far* from the embedded pattern it is still able to retrieve it.

This question can be answered positively [50], [108] by presenting a general scheme in order to express the mutual information as a function of the relevant macroscopic parameters like, e.g., overlap with the embedded patterns, activity, ... and constructing a hamiltonian from it for general Q -state neural networks. For $Q = 2$, one finds back the Hopfield model for biased patterns ensuring that this hamiltonian is optimal in the sense described above. For $Q = 3$, one obtains a Blume-Emery-Griffiths (BEG) type hamiltonian [50] named after the BEG spin-glass [17].

This BEG-model for a FC architecture can then be described as follows. Consider a neural network consisting of N neurons which can take values $\sigma_i, i = 1, \dots, N$ from the discrete set $\mathcal{S} \equiv \{-1, 0, +1\}$. The $p = \alpha N$ patterns to be stored in this network are supposed to be i.i.d.r.v., $\{\xi_i^\mu\}, \mu = 1, \dots, p$ with a probability distribution

$$p(\xi_i^\mu) = \frac{a}{2}\delta(\xi_i^\mu - 1) + \frac{a}{2}\delta(\xi_i^\mu + 1) + (1 - a)\delta(\xi_i^\mu) \quad (52)$$

with a the activity of the patterns so that

$$\lim_{N \rightarrow \infty} \frac{1}{N} \sum_i (\xi_i^\mu)^2 = a. \quad (53)$$

(We remark that for reasons of convenience the pattern activity in this Section is now indicated with a and not with A as in the Q -Ising Section.)

Given the network configuration at time t , $\boldsymbol{\sigma}_N(t) \equiv \{\sigma_j(t)\}, j = 1, \dots, N$, the following dynamics is considered. The configuration $\boldsymbol{\sigma}_N(0)$ is chosen as input. All neurons are updated in parallel according to the rule (7) at zero temperature or the transition probability (5) at arbitrary temperature. But, here the energy potential $\epsilon_i[s|\boldsymbol{\sigma}_N(t)]$ is different from (6) and defined by

$$\epsilon_i(s|\boldsymbol{\sigma}_N(t)) = -s h_i(\boldsymbol{\sigma}_N(t)) - s^2 \theta_i(\boldsymbol{\sigma}_N(t)), \quad (54)$$

where the following local fields in neuron i carry all the information

$$h_{N,i}(t) = \sum_{j \neq i} J_{ij} \sigma_j(t), \quad \theta_{N,i}(t) = \sum_{j \neq i} K_{ij} \sigma_j^2(t) \quad (55)$$

with the obvious shorthand notation for the local fields. The synaptic couplings J_{ij} and K_{ij} are of the Hebb-type

$$J_{ij} = \frac{1}{a^2 N} \sum_{\mu=1}^p \xi_i^\mu \xi_j^\mu, \quad K_{ij} = \frac{1}{N} \sum_{\mu=1}^p \eta_i^\mu \eta_j^\mu \quad (56)$$

with

$$\eta_i^\mu = \frac{1}{a(1-a)} ((\xi_i^\mu)^2 - a). \quad (57)$$

The first part is the usual rule in a three-state network (recall Section 2.1) that codifies the patterns, while the second part can be considered as codifying the fluctuations of the binary active patterns $(\xi_i^\mu)^2$ about their average. That part is also consistent with the modified Hebb rule for the Hopfield model with biased patterns. The updating rule (7) is equivalent to using a gain function

$$\sigma_i(t+1) = g(h_{N,i}(t), \theta_{N,i}(t)) = \text{sign}(h_{N,i}(t)) \Theta(|h_{N,i}(t)| + \theta_{N,i}(t)) \quad (58)$$

with Θ the Heaviside function.

The order parameters of this system have been obtained starting from the mutual information as a measure for the retrieval quality of the system [50], [108]. They are the retrieval overlap, the activity overlap, and the neural activity

$$\begin{aligned} m_N^\mu(t) &= \frac{1}{aN} \sum_i \xi_i^\mu \sigma_i(t), & n_N^\mu(t) &= \frac{1}{aN} \sum_i (\xi_i^\mu)^2 (\sigma_i(t))^2, \\ q_N(t) &= \frac{1}{N} \sum_i (\sigma_i(t))^2. \end{aligned} \quad (59)$$

(We remark that in this Section the neural activity is now denoted by q instead of a .) Instead of using the activity overlap $n_N^\mu(t)$ itself it is more convenient to employ the modified activity overlap

$$l_N^\mu(t) = \frac{1}{1-a} (n_N^\mu(t) - q_N(t)) = \frac{1}{N} \sum_i (\eta_i^\mu) (\sigma_i(t))^2. \quad (60)$$

This parameter can also be called fluctuation overlap since it can be viewed as the retrieval overlap between the binary states $\sigma_i^2(t)$ and the patterns $\eta_i^\mu(t)$. It is, in general, independent of the retrieval overlap $m^\mu(t)$. It gives rise to new states, the so-called quadrupolar (or pattern-fluctuation retrieval) states with $m = 0$ but $l \neq 0$. These states have a retrieval overlap zero but the activity overlap is not, meaning that the active neurons (± 1) coincide with the active patterns but the signs are not correlated. Hence they carry some retrieval information and they might be important in practical applications. In pattern recognition, e.g., looking at a black and white picture on a grey background, these states would describe the situations where the exact location of the picture with respect to the background is known but, the details of the picture itself are not focused. Furthermore, these states might be helpful in modelling such focusing problems discussed in the framework of cognitive neuroscience [6].

The long-time behaviour of this network is governed by the following Hamiltonian [50], [108], precisely obtained by optimizing the mutual information

$$H = -\frac{1}{2} \sum_{i \neq j} J_{ij} \sigma_i \sigma_j - \frac{1}{2} \sum_{i \neq j} K_{ij} \sigma_i^2 \sigma_j^2. \quad (61)$$

Since we want to compare this model with the 3-Ising model and we want to be able to change the relative importance of the two terms we rewrite the Hamiltonian as

$$H = -\frac{A}{2} \sum_{i \neq j} \tilde{J}_{ij} \sigma_i \sigma_j - \frac{B}{2} \sum_{i \neq j} \tilde{K}_{ij} \sigma_i^2 \sigma_j^2, \quad (62)$$

with

$$\tilde{J}_{ij} = aJ_{ij}, \quad \tilde{K}_{ij} = a(1-a)K_{ij}. \quad (63)$$

For

$$A = \frac{1}{a}, \quad B = \frac{1}{a(1-a)} \quad (64)$$

we trivially recover the model above. When we now take $K_{ij} = b\delta_{ij}$ and $A = B = 1$ we obtain the 3-state Ising model (recall eq.(45)). Finally, we find back the Hopfield model by taking first $B = 0$ and then $a = 1$, again with $A = 1$.

For the ED and LF architectures we have to adapt the Hebbian learning rule (56) analogously as in the Q -Ising model. For the ED case both Hebbian weights are multiplied with the factor $c_{ij}N/C$, where we recall that c_{ij} is a random variable assuming values 0 and 1 with mean $C \approx O(\ln N/N)$. For the LF architecture we consider

$$J_{ij}(t) = \frac{1}{a^2N} \sum_{\mu=1}^p \xi_i^\mu(t+1)\xi_j^\mu(t), \quad K_{ij}(t) = \frac{1}{N} \sum_{\mu=1}^p \eta_i^\mu(t+1)\eta_j^\mu(t). \quad (65)$$

We remark that an underlying assumption that leads to the BEG model and that should be preserved in any implementation is that the dynamic activity $q \approx a$, as far as the order of magnitude is concerned.

3.2 Solving the dynamics

The discussion given in Section 2.2 on the correlations appearing for the various architectures remains valid for this model. Furthermore, the development of the recursive scheme presented there can be followed in order to study the time evolution of the distribution of the local fields $h_i(t)$ and $\theta_i(t)$. This allows one to write down recursion relations determining the full time evolution of the order parameters (59)-(60) of the model.

Since the method has been explained already in some detail in Section 2.2 and the explicit analysis is even more technical we do not write it out here. For the FC architecture we refer to [58] for the treatment at zero temperature and to [59] for an extension to arbitrary temperatures. The final results are two recursion relations of the type studied in Section 2.2.3, one for $h_i(t)$ and one for $\theta_i(t)$.

Also for the BEG network the first few time steps of its evolution have been worked out analytically and have been compared with numerical simulations for systems up to $N = 7000$ neurons averaged over 500 runs. As an illustration we refer to fig. 4 left presenting the order parameter l as a function of α for uniform patterns and initial conditions $m_0 = l_0 = 0.6$, $q_0 = 0.5$ and $T = 0.5$. We remark that the maximal capacity for this system is $\alpha_c \simeq 0.06$ ([74]). We then learn that

the first time steps agree very well and do give a reasonable estimate of the critical capacity.

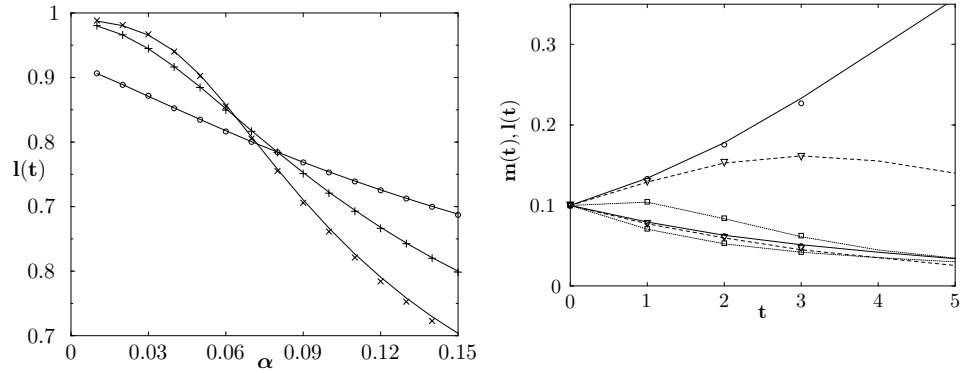


Figure 4: The BEG model on a FC architecture with uniform patterns. Left: Order parameter $l(t)$ as a function of the capacity α for the first three time steps with initial conditions $m_0 = l_0 = 0.6, q_0 = 0.5$ at $T = 0.5$. Theoretical results (solid lines) versus simulations (time 1, 2 and 3 represented by a circle, a plus respectively a times symbol) are shown. Right: Order parameters $m(t)$ (bottom three lines) and $l(t)$ (top three lines) as a function of time with initial conditions $m_0 = l_0 = 0.1, q_0 = 0.5$ at $T = 1.1$ and several values of α . Theoretical results (open symbols) versus simulations (full lines for $\alpha = 0.001$, dashed lines for $\alpha = 0.01$ and dotted lines for $\alpha = 0.1$).

In fig. 4 we examine the order parameters m and l in the quadrupolar phase ($m = 0, l > 0$) versus the paramagnetic phase ($m = 0, l = 0$), for several values of α . We see that a few time steps do give us already the characteristic behaviour. When time increases m decreases while l differentiates between the phases, as is seen in the theoretical results as well as in the simulations. For the quadrupolar phase ($\alpha = 0.001$) l increases, deep inside the paramagnetic phase ($\alpha = 0.1$) l decreases, while in the intermediate region ($\alpha = 0.01$) the rate of increase of l quickly diminishes and l itself goes to zero.

At this point, we remark that there is a small but visible discrepancy between the theory and simulations especially in $l(3)$. It is of the order $O(10^{-3})$ and attributed to finite-size effects. This, and the fact that the signal-to-noise approach does not give a closed form solution of the dynamics, has been a motivation to look at the generating functional approach to solve this dynamics. An extensive report is beyond the scope of the present review. Essentially it turns out [59] that beyond the third time step of the dynamics the signal-to-noise analysis as used above is not entirely correct for those parameters of the system corresponding to spin-glass behaviour. The reason is that the technical assumption after eq. (30) is not valid in the spin-glass region but it seems to have little effect in most of the retrieval region

of the networks [59] (and [67] for full details in the simpler case of the Hopfield model).

To confirm this some further numerical experiments have been done for different values of the model parameters comparing this limiting normal distribution (recall eq. (30)) with simulations for different time steps. A comparison for time steps $t = 2$ and $t = 9$ for systems with $N = 2000$ neurons averaged over 250 runs for the initial conditions $m_0 = l_0 = 0.6, q_0 = 0.5, a = 2/3$ and temperature $T = 0.2$ as a function of α shows that in the retrieval region ($\alpha_c < 0.086$) the simulation results coincide quite well with the limiting distribution, while in the spin-glass region, certainly from $\alpha \sim 0.11$ onwards, the results for $t = 9$ start diverting systematically [59]. We remark that the signal to noise approach can be used correctly by refining that technical assumption allowing for the inclusion of all feedback correlations [67].

Concerning the other architectures we mention again that the AED and LF models can be solved exactly [50], [51], [56], [109], and we study the stationary limit in the next subsection. Results on the BEG model with variable dilution, hence, including SED can be found in [96].

3.3 Thermodynamic and retrieval properties

Stationary results for the AED and LF architectures are obtained immediately through the dynamical approach discussed in the previous Section 3.2.

The stationary states of the AED network dynamics are shown in Fig.5, for a typical activity of $a = 0.8$ and $q \sim a$. The pattern activity is chosen somewhat larger than $a = 2/3$ (uniform patterns) since for finite loading $\alpha = 0$ it is easy to find out that the quadrupolar state only exists for $a \geq 0.698$. In addition to the retrieval and quadrupolar phases, $R(m \neq 0, l \neq 0)$ and $Q(m = 0, l \neq 0)$, there is a self-sustained activity phase $S(m = 0, l = 0)$, also referred to as the zero phase Z [50], [109]. We remark that the saddle-points have one-dimensional basins of attraction with attractor directions along l , either towards $l^* \neq 0$ or to $l^* = 0$ and repeller directions along m away from $m = 0$. Furthermore, at the boundary of the maximal storage capacity α_c , both overlaps, m and l , disappear.

A similar behaviour appears for other big values of the pattern activity a , whereas for small a there are only R and S phases. The reason for a low- T retrieval phase and the absence of a Q phase is that a finite T is needed for the active neurons (± 1) to coincide with the active patterns but with uncorrelated signs, such that $m = 0$.

Again a lot of detailed results are available. The most important ones can be summarized as follows. Above the threshold $(\alpha, T) = (0.22, 0.45)$ a stable Q phase starts to appear. For T below that threshold m and l remain finite together,

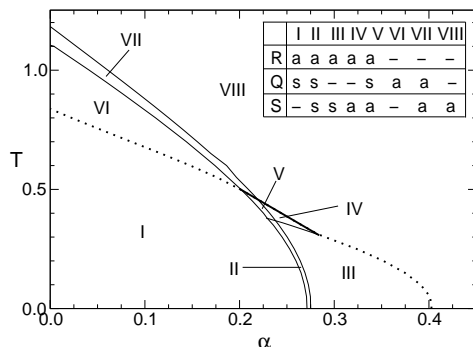


Figure 5: The (T, α) phase diagram for the AED BEG network with pattern activity $\alpha = 0.8$. Full (dotted) thin lines denote discontinuous (continuous) transitions, thick lines denote the boundary of the R phase. The lines at the most right yield the maximal storage capacity. The structure of the retrieval dynamics is explained: a denotes an attractor, s a saddle point, r a repellor.

in a behaviour characteristic for retrieval, up to the maximal α_c . In this regime the fluctuation overlap does not yield anything essentially new that is not contained in the retrieval overlap. In contrast, above the threshold, m disappears first with increasing α leaving a finite $l \neq 0$ up to a bigger α_c . Hence, first T and then α have to become large enough for the Q states to appear. Note that the fluctuation overlap carries a finite information even with $m = 0$ in the Q phase. Thus, although the information transmitted by the network is mainly in the retrieval phase, there is also some information due to the Q phase.

For small α , the fluctuation overlap “drives” a vanishingly small initial retrieval overlap, meaning almost no recognition of a given pattern by the network, into an asymptotic state with finite recognition. This is in contrast with the results for other three-state networks where first the overlap $m(t)$ becomes non-zero: $m(t)$ drives $l(t)$. Furthermore, with a vanishing initial m_0 , the states of the network pass through the vicinity of a saddle point Q , with a finite fluctuation overlap l and still a vanishing retrieval overlap at small or intermediate times, giving some plateaus in q , l and the information content. It is only in passing beyond those plateaus, which may take a rather long time, that the states attain the asymptotic behaviour of the retrieval phase.

In general, the basins of attraction for retrieval and the information content are larger in the BEG network than in other three-state networks. These results for the dynamics and the stationary states are confirmed by flow diagrams [51], [109].

For the LF architecture some typical phase diagrams are shown in Fig. 6. We first remark that we need to introduce two further variables in the derivation of the

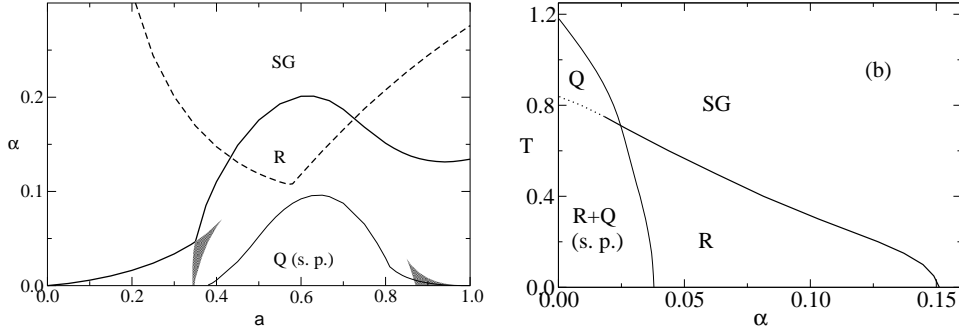


Figure 6: The (α, a) , $T = 0$ (left) and (T, α) , $a = 0.8$ (right) phase diagram for the LF BEG network. There is a SG solution everywhere. There is a stable R phase (a second one with a smaller overlap in the shaded area) below the thick full line. Left: The Q state appears as a saddle-point below the thin full line. The thick dashed line shows the retrieval phase boundary for the optimal LF $Q = 3$ -Ising model. Right: There is a stable (saddle-point) Q phase above (below) the thick (dotted) line, ending discontinuously at the full thin line.

LF recurrence relations for the variances of the two noises i.e.

$$q_1(t) = \left\langle \left\langle \sigma_i(t) \right\rangle_{\beta}^2 \right\rangle_{\{\xi^{\mu}\}}, \quad p_1(t) = \left\langle \left\langle \sigma_i^2(t) \right\rangle_{\beta}^2 \right\rangle_{\{\xi^{\mu}\}}. \quad (66)$$

The possible phases are then $R(m > 0, l > 0, q_1 > 0, q_0 > 0)$, $Q(m = 0, l > 0, q_1 > 0, q_0 > 0)$ and $SG(m = 0, l = 0, q_1 > 0, q_0 > 0)$. From Fig. 6 we notice that a stable Q phase only appears for sufficiently large T and large a , a feature already seen for the AED architecture. Thus, as T increases, the useful performance of the network goes over from the retrieval to the pattern-fluctuation retrieval phase. Furthermore, we see that for intermediate activity $a \in (0.435, 0.727)$ the LF BEG network has a bigger maximal storage capacity than the optimal LF Ising network [53], optimal in the sense that the adjustable threshold parameter was chosen to optimize the storage capacity α . The same has been found for the information content. At larger activity, $a = 0.8$ say, the BEG and Ising networks compete for better performance at intermediate or larger α values. Moreover, as in the AED architecture, the flows to the stable solutions are considerably delayed by the saddle points in the form of slow transients of the dynamics. Finally, a remarkable feature is the presence of quite large basins of attraction either to the stable R state or to the stable Q state, even for the fairly high T (and small α). Also, not surprisingly, one finds a much smaller basin of attraction to the SG states. Similar features have also been found in the dynamics of the AED network except for the SG states, which are absent in that case.

For the symmetric architectures we restrict ourselves here to the FC one. Results on the architecture with variable dilution can be found in [96]. We apply directly the standard replica technique in order to calculate the free energy of the model. Within the replica-symmetry approximation and for a finite number, s , of condensed patterns, we obtain

$$\begin{aligned}
f(\beta) &= \frac{1}{2} \sum_{\mu=1}^s \left(aA m_\mu^2 + a(1-a)B l_\mu^2 \right) + \frac{\alpha}{2\beta} \log(1-\chi) + \frac{\alpha}{2\beta} \log(1-\phi) \\
&+ \frac{\alpha}{2\beta} \frac{\chi}{1-\chi} + \frac{\alpha}{2\beta} \frac{\phi}{1-\phi} + \frac{\alpha}{2} \frac{Aq_1\chi}{(1-\chi)^2} + \frac{\alpha}{2} \frac{Bp_1\phi}{(1-\phi)^2} \\
&- \frac{1}{\beta} \left\langle \int DsDt \ln \text{Tr}_\sigma \exp(\beta \tilde{H}) \right\rangle_{\{\xi^\mu\}}, \tag{67}
\end{aligned}$$

with the effective Hamiltonian \tilde{H} given by

$$\begin{aligned}
\tilde{H} &= A\sigma \left[\sum_{\mu} m_{\mu} \xi^{\mu} + \sqrt{\alpha r s} \right] + B\sigma^2 \left[\sum_{\mu} l_{\mu} \eta^{\mu} + \sqrt{\alpha u t} \right] \\
&+ \frac{\alpha}{2} \frac{A\chi}{1-\chi} \sigma^2 + \frac{\alpha}{2} \frac{B\phi}{1-\phi} \sigma^2. \tag{68}
\end{aligned}$$

Here

$$\chi = A\beta(q_0 - q_1), \quad \phi = B\beta(p_0 - p_1), \quad r = \frac{q_1}{(1-\chi)^2}, \quad u = \frac{p_1}{(1-\phi)^2}. \tag{69}$$

In these expressions the relevant order parameters are

$$m_{\mu} = \frac{1}{a} \left\langle \xi^{\mu} \int DsDt \langle \sigma \rangle_{\beta} \right\rangle_{\{\xi^{\mu}\}}, \tag{70}$$

$$l_{\mu} = \frac{1}{a(1-a)} \left\langle \eta^{\mu} \int DsDt \langle \sigma^2 \rangle_{\beta} \right\rangle_{\{\xi^{\mu}\}}, \tag{71}$$

$$q_0 = p_0 = \left\langle \int DsDt \langle \sigma^2 \rangle_{\beta} \right\rangle_{\{\xi^{\mu}\}}, \tag{72}$$

$$q_1 = \left\langle \int DsDt \langle \sigma \rangle_{\beta}^2 \right\rangle_{\{\xi^{\mu}\}}, \tag{73}$$

$$p_1 = \left\langle \int DsDt \langle \sigma^2 \rangle_{\beta}^2 \right\rangle_{\{\xi^{\mu}\}}, \tag{74}$$

where $\langle \cdot \rangle_{\beta}$ represents the thermal average with respect to \tilde{H} . As usual we take only one condensed pattern such that the index μ can be dropped. The parameters

q_1 and p_1 are the Edwards-Anderson order parameters with their conjugate variables r respectively u . Finally, χ and ϕ are the susceptibilities proportional to the fluctuation of the m overlap, respectively l overlap. All these parameters are the stationary limits of the corresponding parameters considered in the dynamics for arbitrary temperatures. We remark that the trace over the neurons and the average over the patterns can be performed explicitly. The resulting expressions are written down in [74] and have been solved numerically.

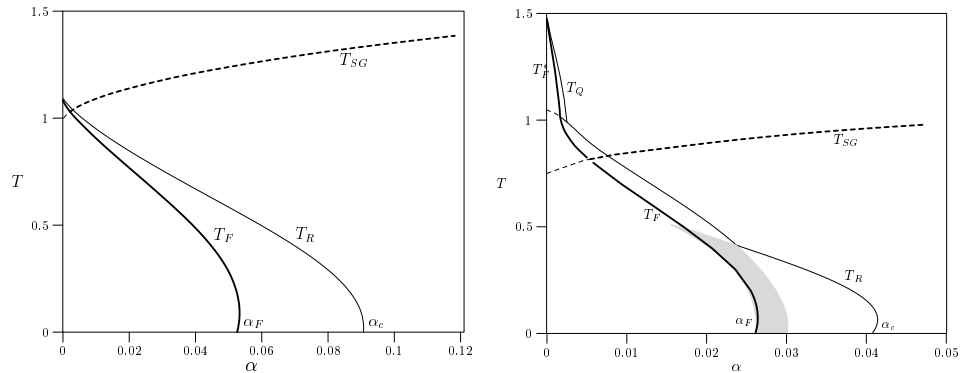


Figure 7: The BEG ($\alpha - T$) phase diagram for $a = 2/3$ (left) and $a = 0.8$ (right). Dashed lines correspond to continuous transitions, while full lines correspond to discontinuous transitions (in all order parameters). Below the line T_R retrieval states occur. The curve T_F represents the thermodynamic transition (shown as a thick line) between retrieval states and spin-glass states. The line T_{SG} denotes the transition from the spin-glass to the paramagnetic phase. Below the line T_Q quadrupolar states exist and below the line T_F^* they are global minima. In the shaded region two retrieval states coexist.

From fig. 7 (left) for uniform patterns and a comparison with the results for the FC $Q = 3$ -Ising model (cfr. fig 2 right) one learns that $\alpha_c = 0.091$ is almost double of the maximal capacity for the latter, $\alpha_c = 0.046$, in the case of an optimal choice for the gain parameter b , i.e. $b = 1/2$. Compared with the Hopfield model, one sees that α_c is smaller in the BEG model, 0.091 versus 0.13, but α_F is larger, 0.053 versus 0.051. So a bigger number of the retrieval states in the BEG network are global minima of the free energy. Finally, one also notices that the critical curves T_{SG} and T_R end in different temperature points at $\alpha = 0$ giving rise to a ‘crossover’ region for small α as it typically occurs in other multi-state models, e.g., the Potts model [110], [111] and the Askin-Teller model [79]. This is related with the fact that for $\alpha = 0$ these models have a discontinuous transition at T_F . In this crossover region the retrieval states (global minima below T_F) and the paramagnetic states (local minima below T_F) coexist.

As in the AED and LF architecture the quadrupolar phase is situated in the high

temperature region and we can understand the physics behind it in the following way. The spin-glass order parameter q_1 is zero, meaning that the ± 1 spins are not frozen and as a consequence m can be zero. The fact that l is not zero practically means that the spins can flip freely between ± 1 but the probability that they jump to 0 or vice versa becomes very small. This effect arises from $a > 1/2$ onwards when the ratio between the second and the first term in the Hamiltonian starts increasing as $(1 - a)^{-1}$. It implies that the information content of the system is non-zero in this phase.

Finally, we recall that for $\gamma \equiv a(1 - a)B = 1$ (cfr. eq. (61)–(64)), we recover the BEG neural network as studied above. However, it turns out that the maximum in the capacity is located at $\gamma = 0.712$ with a corresponding value of $\alpha_c = 0.096$. A reason for this is the approximation $q_0 \sim a$ made in order to get the mean-field Hamiltonian. The mutual information of the network is optimized under this assumption but, in general, it may not be completely realized in a specific model. Furthermore, the fact that replica-symmetry breaking may be bigger for larger α , as is also indicated by the zero-temperature entropy calculation, could be an extra reason for this. For more details we refer to the literature mentioned above.

4 The Gardner capacity of multi-state models

In the previous Section it has been found that the capacity and basin of attraction of the BEG network have been enlarged in comparison with those of other three-state networks. The models considered all have Hebbian-type learning rules. A natural question is then whether these improved retrieval quality aspects are restricted to the use of the Hebb rule or whether they are an intrinsic property of the BEG model. Therefore, we want to answer the following: given the set of p patterns specified above, is there a network (the best possible network of the BEG-type) which has these patterns as fixed points of the deterministic form of the dynamics (58)?

In order to do so we consider the perceptron architecture (N inputs with couplings J_j and K_j and 1 output) and we say that a given pattern, $\xi_i^\mu, i = 1, \dots, N$, is stored if there exists a corresponding output ξ_0^μ

$$\xi_0^\mu = g(h^\mu, \theta^\mu) \quad (75)$$

with

$$h^\mu = \frac{1}{\sqrt{N}} \sum_{j=1}^N J_j \xi_j^\mu \quad \theta^\mu = \frac{1}{\sqrt{N}} \sum_{j=1}^N K_j (\xi_j^\mu)^2, \quad (76)$$

and $\{\mathbf{J}, \mathbf{K}\} \equiv \{J_j, K_j\}$ denoting the configurations in the space of interactions. The factor $N^{-1/2}$ is introduced to have the weights J_j and K_j of order unity (spherical constraint).

The aim is then to determine the maximal number of patterns, p , that can be stored in the perceptron, in other words to find the maximal value of the loading $\alpha = p/N$ for which couplings satisfying (75)-(76) can still be found. Following a Gardner-type analysis [21] the fundamental quantity that we want to calculate is then the volume fraction of weight space given by

$$V = \int d\mathbf{J}d\mathbf{K}\rho(\mathbf{J}, \mathbf{K}) \prod_{\mu=1}^p \chi_{\xi_0^\mu}(h^\mu, \theta^\mu; \kappa) \quad (77)$$

with the characteristic function

$$\begin{aligned} \chi_{\xi_0^\mu}(h^\mu, \theta^\mu; \kappa) &= \delta_{\xi_0^\mu, g(h^\mu, \theta^\mu)} \\ &= (\xi_0^\mu)^2 \Theta(|h^\mu| + \theta^\mu - \kappa) \Theta(\xi_0^\mu h^\mu - \kappa) \\ &\quad + (1 - (\xi_0^\mu)^2) \Theta(-|h^\mu| - \theta^\mu - \kappa) \end{aligned} \quad (78)$$

where κ is the imbedding stability parameter measuring the size of the basin of attraction for the μ -th pattern and $\rho(\mathbf{J}, \mathbf{K})$ is the following normalization factor assuming spherical constraints for the couplings

$$\rho(\mathbf{J}, \mathbf{K}) = \frac{\delta(\mathbf{J} \cdot \mathbf{J} - N)\delta(\mathbf{K} \cdot \mathbf{K} - N)}{\int_{-\infty}^{\infty} d\mathbf{J}d\mathbf{K}\delta(\mathbf{J} \cdot \mathbf{J} - N)\delta(\mathbf{K} \cdot \mathbf{K} - N)}. \quad (79)$$

In order to perform the average over the disorder in the input patterns and the corresponding output we employ the replica technique to evaluate the entropy per site

$$v = \lim_{N \rightarrow \infty} \frac{1}{N} \langle \ln V \rangle \quad (80)$$

where $\langle \langle \cdot \rangle \rangle$ denotes an average over the statistics of inputs $\{\xi_j^\mu\}$ and outputs $\{\xi_0^\mu\}$, recalling (52).

In the replica approach the entropy per site v is computed via the expression

$$v = \lim_{N \rightarrow \infty} \lim_{n \rightarrow 0} \frac{1}{nN} (\langle \langle V^n \rangle \rangle - 1) = \lim_{N \rightarrow \infty} \lim_{n \rightarrow 0} \frac{1}{nN} \ln \langle \langle V^n \rangle \rangle \quad (81)$$

where V^n is the n -times replicated fractional volume

$$\begin{aligned} \langle \langle V^n \rangle \rangle &\propto \int \left[\prod_{\alpha=1}^n d\mathbf{J}^\alpha d\mathbf{K}^\alpha \delta(\mathbf{J}^\alpha \cdot \mathbf{J}^\alpha - N) \delta(\mathbf{K}^\alpha \cdot \mathbf{K}^\alpha - N) \right] \\ &\quad \times \left\langle \left\langle \prod_{\alpha=1}^n \prod_{\mu=1}^p \chi_{\xi_0^\mu}(h_\mu^\alpha, \theta_\mu^\alpha; \kappa) \right\rangle \right\rangle \end{aligned} \quad (82)$$

whereby we can forget, since the couplings are continuous, about constant terms such as the denominator in (79). The replica-symmetric calculation then proceeds in a standard way, although the technical details are much more complicated, and an analytic formula can be obtained [77].

Comparing with analogous discussions in the literature for other three-state neuron perceptron models we recall that for $\kappa = 0$ and uniform patterns the $Q = 3$ Ising perceptron can maximally reach an optimal capacity equal to 1.5, depending on the separation between the plateaus of the gain function (see [75], [76] for the precise details) and the $Q = 3$ clock and Potts model both reach an optimal capacity of 2.40 [112], [113] while the value for the BEG perceptron found here is 2.24. Here we have to recall that the $Q = 3$ Ising perceptron and the BEG perceptron have the same topology structure in the neurons, whereas the $Q = 3$ clock and Potts models have a different topology, as explained in the Introduction. Since, in general, perceptrons turn out to be very useful models in connection with learning and generalization this is an interesting observation.

The stability of the replica-symmetric solution has been studied by generalizing the de Almeida-Thouless analysis and deriving an analytic expression for the *two* replicon eigenvalues that play a role in the Gardner limit. Breaking only occurs for small activities and very small imbedding constants, $\kappa < 0.0061$. This is consistent with the stability results found for the $Q = 3$ Ising perceptrons.

These results strenghten the idea that the better retrieval properties found for the BEG model in comparison with the $Q = 3$ Ising model are not restricted to the specific Hebb rule but are intrinsic to the model.

5 Concluding remarks

In this overview we have studied the dynamics and retrieval properties of multi-state neural networks based upon spin-glass models. In particular, we have first discussed the Q -Ising model and the Blume-Emery-Griffiths model with various architectures and Hebbian-type learning rules. The methods used are the signal-to-noise analysis and the thermodynamic mean-field replica technique. Then, the Gardner optimal capacity for these models has been considered.

A number of detailed results have been outlined in order to compare the properties of the different networks and architectures. The Blume-Emery-Griffiths model, obtained by maximizing the mutual information content of networks with scalar valued three-state neurons, shows improved retrieval properties in comparison with the $Q = 3$ -Ising model.

Acknowledgments

This work has been supported in part by the Fund for Scientific Research, Flanders-Begium. The author is indebted to S. Amari, J. Busquets Blanco, D. Carlucci, D. Dominguez, R. Erichsen Jr., J. Huyghebaert, G. Jongen, E. Korutcheva, P. Kozlowski, R. Kühn, I. Pérez Castillo, H. Rieger, G.M. Shim, W.K. Theumann, J. van Mourik, T. Verbeiren, B. Vinck, K.Y.M. Wong and V. Zagrebnov for pleasant collaborations on some of these subjects during previous years. He especially thanks T. Verbeiren for discussions about the present text.

References

- [1] D. Bollé, G. Jongen and G.M. Shim, in *Mathematical Physics and Stochastic Analysis*, eds. S. Albeverio et al. World Scientific, Singapore, 2000, p. 114
- [2] D. Bollé, G. Jongen and G.M. Shim, *J. Stat. Phys.* **91**, 125 (1998).
- [3] D. Bollé, B. Vinck, and V.A. Zagrebnov, *J. Stat. Phys.* **70**, 1099 (1993).
- [4] T. Tadaki and J. Inoue, *Phys. Rev. E* **65**, 016101 (2001).
- [5] J. Inoue and D.M. Carlucci, *Phys. Rev. E* **64**, 036121 (2001).
- [6] D.L. Schacter, K.A. Norman and W. Koutstaal, *Annu. Rev. Psychol.* **49**, 289 (1998).
- [7] H. Komatsu and Y. Ideura, *J. Neurophysiol.* **70**, 677 (1993).
- [8] L.R. Squire, *Science* **232**, 1612 (1986).
- [9] J.J. Hopfield, *Proc. Nat. Acad. Sci. USA* **79**, 2554 (1982).
- [10] J.J. Hopfield, *Proc. Nat. Acad. Sci. USA* **81**, 3088 (1984).
- [11] D.J. Amit, H.G. Gutfreund and H. Sompolinsky, *Ann. Phys. NY* **173**, 30 (1987).
- [12] D. Sherrington and S. Kirkpatrick, *Phys. Rev. Lett.* **35**, 1792 (1972).
- [13] S.K. Ghatak and D. Sherrington, *J. Phys. C* **10**, 3149 (1977).
- [14] F.D. Nobre and D. Sherrington, *J. Phys. C* **19**, L181 (1986).
- [15] D. Elderfield and D. Sherrington, *J. Phys. C* **16**, L497 (1983).

- [16] F.D. Nobre and D. Sherrington, *J. Phys. A* **26**, 4593 (1993).
- [17] J. M. de Araújo, F. A. da Costa and F. D. Nobre, *Eur. Phys. J. B* **14**, 661 (2000).
- [18] E. Barkai, I. Kanter and H. Sompolinsky, *Phys. Rev. A* **41**, 590 (1990).
- [19] D.O. Hebb, *The organization of behaviour*, Wiley, New York, 1949.
- [20] R. Penrose, *Cambridge Philos. Soc.* **51**, 406 (1955); **52**, 17 (1956).
- [21] E. Gardner, *Europhys. Lett.* **4**, 481 (1987); *J. Phys. A* **21**, 257 (1988).
- [22] E. Gardner and B. Derrida, *J. Phys. A* **21**, 271 (1988).
- [23] D.J. Amit, *Modeling brain function. The world of attractor neural networks*, Cambridge Univ. Press, 1989.
- [24] J. Hertz, A. Krogh and R.G. Palmer, *Introduction to the theory of neural computation*, Addison-Wesley, Redwood City, 1991.
- [25] P. Peretto, *An introduction to the modeling of neural networks*, Cambridge Univ. Press, 1992.
- [26] V. Dotsenko, *The theory of spin glasses and neural networks*, World Scientific, Singapore, 1994.
- [27] B. Müller, J. Reinhardt and M.T. Strickland, *Neural networks: An introduction*, Springer, Berlin, 2nd edition 1995.
- [28] H. Nishimori, *Statistical Physics of spin glasses and information processing*, Oxford Univ. Press, 2001.
- [29] A. Engel and C. Van den Broeck, *Statistical mechanics of learning*, Cambridge Univ. Press, 2001.
- [30] E. Domany, J.L. van Hemmen and K. Schulten, eds. *Models of neural networks*, Springer, Berlin, 1991.
- [31] E. Domany, J.L. van Hemmen and K. Schulten, eds. *Models of neural networks II: Temporal aspects of coding and information processing in biological systems*, Springer, Berlin, 1994.
- [32] E. Domany, J.L. van Hemmen and K. Schulten, eds. *Models of neural networks III: association, generalization and representation*, Springer, Berlin, 1996.

- [33] D. Saad, ed. *On-line learning in neural networks*, Cambridge Univ. Press, 1998.
- [34] W. Kinzel, *Z. Phys. B* **60**, 205 (1985).
- [35] S. Amari and K. Maginu, *Neural Networks* **1**, 63 (1988).
- [36] H. Nishimori and T. Ozeki, *J. Phys. A* **26**, 859 (1993).
- [37] M. Okada, *Neural Networks* **8**, 833 (1995).
- [38] R.D. Henkel and M. Opper, *Europhys. Lett.* **11**, 403 (1990).
- [39] M. Shiino and T. Fukai, *Phys. Rev. E* **48**, 867 (1993).
- [40] A.E. Patrick and V.A. Zagrebnov, *J. Stat. Phys.* **63**, 59 (1991).
- [41] A.E. Patrick and V.A. Zagrebnov, *J. Phys. A* **24**, 3413 (1991).
- [42] B. Derrida, E. Gardner, and A. Zippelius, *Europhys. Lett.* **4**, 167 (1987).
- [43] J.S. Yedidia, *J. Phys. A* **22**, 2265 (1989).
- [44] M. Bouten and A. Engel, *Phys. Rev. E* **47**, 1397 (1993).
- [45] D. Bollé, G.M. Shim, B. Vinck, and V.A. Zagrebnov, *J. Stat. Phys.* **74**, 565 (1994).
- [46] D.R.C. Dominguez and W.K. Theumann, *J. Phys. A* **29**, 749 (1996).
- [47] D.R.C. Dominguez and D. Bollé, *Phys. Rev. E* **56**, 7306 (1997).
- [48] R. Erichsen Jr. and W. K. Theumann, *Phys. Rev. E* **59**, 947 (1999).
- [49] Y. Nakamura and A.R. Ferchmin, *Eur. Phys. J.* **13**, 305 (2000).
- [50] D.R.C. Dominguez and E. Korutcheva, *Phys. Rev. E* **62**, 2620 (2000).
- [51] D. Bollé, D. R.C. Dominguez, R. Erichsen Jr., E. Korutcheva and W.K. Theumann, cond-mat/0208281.
- [52] E. Domany, W. Kinzel, and R. Meir, *J. Phys. A* **22**, 2081 (1989).
- [53] D. Bollé, G.M. Shim, and B. Vinck, *J. Stat. Phys.* **74**, 583 (1994).
- [54] G.M. Shim, K.Y.M. Wong and D. Bollé, *J. Phys. A* **30**, 2637 (1997).
- [55] D.R.C. Dominguez and W.K. Theumann, *J. Phys. A* **30**, 1403 (1997).

- [56] D. Bollé, R. Erichsen Jr. and W.K. Theumann, cond-mat/0305587.
- [57] C. Meunier, D. Hansel and A. Verga, J. Stat. Phys **35**, 859 (1989).
- [58] D. Bollé, J. Busquets Blanco and G.M. Shim, Physica A **318**, 613 (2003).
- [59] D. Bollé, J. Busquets Blanco, G.M. Shim and T. Verbeiren, cond-mat/0304553.
- [60] D. Bollé, G. Jongen and G.M. Shim, J. Stat. Phys. **96**, 861 (1999).
- [61] T.L.H. Watkin and D. Sherrington, J. Phys. A **24**, 5427 (1991).
- [62] A.E. Patrick and V.A. Zagrebnov, J. Phys. A **23**, L1323 (1990); J. Phys. A **25**, 1009 (1992).
- [63] W. K. Theumann and R. Erichsen Jr., Phys. Rev. E **64**, 061902 (2001).
- [64] E.D. Siggia, P.C. Martin and H.A. Rose, Phys. Rev. A **8**, 423 (1973).
- [65] C. De Dominicis, Phys. Rev. B **18**, 4913 (1978).
- [66] A.C.C. Coolen, in *Handbook of Biological Physics Vol 4*, ed. by F. Moss and S. Gielen, Elsevier Science B.V. 2001, p. 597
- [67] D. Bollé, J. Busquets Blanco, and T. Verbeiren, The signal-to-noise analysis for the Little-Hopfield model revisited, in preparation.
- [68] M. Mézard, G. Parisi and M.A. Virasoro, *Spin glass theory and beyond*, World Scientific, Singapore, 1987
- [69] H. Rieger, J. Phys. A **23**, L1273 (1990).
- [70] D. Bollé, H. Rieger and G.M. Shim, J. Phys. A **27**, 3411 (1994).
- [71] S. Bös and R. Kühn, J. Stat. Phys. **76**, 1495 (1994).
- [72] R. Erichsen Jr., W. K. Theumann and D.R.C. Dominguez, Phys. Rev. E **60**, 7321 (1999).
- [73] D. Bollé, D. Carlucci and G.M. Shim, J. Phys. A **33**, 6481 (2000).
- [74] D. Bollé and T. Verbeiren, J. Phys. A **36**, 6481 (2003).
- [75] S. Mertens, H.M. Köhler and S. Bös J. Phys. A **24**, 4941 (1991).
- [76] D. Bollé and J. van Mourik, J. Phys. A **27**, 1151 (1994).

- [77] D. Bollé, I. Pérez Castillo and G.M. Shim, Phys. Rev. E **67**, 036113 (2003).
- [78] D. Bollé and P. Kozłowski, J. Phys. A **35**, 2093 (2002).
- [79] D. Bollé and P. Kozłowski, J. Phys. A **32**, 8577 (1999).
- [80] P. Kozłowski, Ashkin-Teller neural network models, Ph.D. thesis, K.U.Leuven, Belgium (2002).
- [81] M. Okada, Neural Networks **9**, 1429 (1996).
- [82] D.R.C. Dominguez and D. Bollé, Phys. Rev. Lett. **80**, 2961 (1998).
- [83] D. Bollé and D.R.C. Dominguez, Physica A **286**, 401 (2000).
- [84] R. Kree and A. Zippelius, in *Models of neural networks*, eds. E. Domany, J.L. van Hemmen and K. Schulten, Springer, Berlin 1991.
- [85] A.N. Shiryayev, *Probability*, Springer, New York, 1984.
- [86] G. Jongen, *On the dynamics of spin-glass models of neural networks*, Ph. D. thesis, K.U.Leuven, Belgium 1999.
- [87] A.E. Patrick and V.A. Zagrebnoy, J. Phys. (Paris) **51**, 1129 (1990).
- [88] B. Derrida, J. Phys. A **20**, L271 (1987).
- [89] B. Derrida and R. Meir, Phys. Rev. A **38**, 3116 (1988).
- [90] D. Bollé, D.R.C. Dominguez and S. Amari, Neural Networks **13**, 455 (2000).
- [91] E. Gardner, B. Derrida and P. Mottishaw, J. Physique **48**, 741 (1987).
- [92] W. Krauth, J.P. Nadal and M. Mézard, J. Phys. A **21**, 2995 (1988).
- [93] H. Horner, D. Bormann, M. Frick, H. Kinzelbach and A. Schmidt, Z. Phys. B **76**, 381 (1989).
- [94] R.D. Henkel and M. Opper J. Phys. A **24**, 2201 (1991).
- [95] D. Gandolfo, M. Sirugue-Collin and V.A. Zagrebnoy, Network: Computation in Neural Systems **9**, 563 (1998).
- [96] T. Verbeiren, Variable dilution in neural networks, Ph. D. thesis, K.U.Leuven, Belgium (2003).
- [97] M. Shiino and T. Fukai, J. Phys. A **25**, L375 (1992).

- [98] D. Bollé and G.M. Shim, Phys. Rev. E **65**, 067101 (2002).
- [99] V.A. Zagrebnov and A.S. Cvyrov, Sov. Phys. JETP **68**, 153 (1989).
- [100] A.C.C. Coolen and D. Sherrington, Phys. Rev. E **49**, 1921 (1994),
- [101] T.L.H. Watkin and D. Sherrington, Europhys. Lett. **14**, 791 (1991).
- [102] A. Canning and J-P. Naef, J. Phys. I France **2**. 1791 (1992)
- [103] L. Viana and A.J. Bray, J. Phys. C **18**, 3037 (1985)
- [104] R. Bidaux, J.P. Carton and G. Sarma, J. Phys. A **9**, L87 (1976).
- [105] J.R.L de Almeida and D.J. Thouless, J. Phys. A **11**, 983, (1987).
- [106] C. E. Shannon, Bell Syst. Techn. J. **27**, 379 (1948).
- [107] R.E. Blahut, *Principles and Practice of Information Theory*, Addison-Wesley, Reading, MA, 1990, Chapter 5.
- [108] D. Bollé and T. Verbeiren, Physics Letters A **297**, 156 (2002).
- [109] D. R. C. Dominguez, E. Korutcheva, W. K. Theumann, and R. Erichsen Jr., in Lecture Notes in Computer Science (Springer, Berlin) **2415**, 129 (2002).
- [110] I. Kanter, Phys. Rev. A **37**, 2739 (1988).
- [111] D. Bollé, P. Dupont and J. Huyghebaert, Phys. Rev. A **45**, 4194 (1992).
- [112] F. Gerl and U. Krey, J. Phys. A **27**, 7353 (1994).
- [113] F. Gerl, K. Bauer and U. Krey, Z. Phys. B **88**, 339 (1992).